PLOS ONE

RESEARCH ARTICLE

Application of the Taguchi method to explore a robust condition of tumor-treating field treatment

Kosaku Kurata[1]*, **Kazuki Shimada**[2], **Hiroshi Takamatsu**[1]

1 Department of Mechanical Engineering, Kyushu University, Fukuoka, Japan, **2** Graduate School of Engineering, Kyushu University, Fukuoka, Japan

* kurata@mech.kyushu-u.ac.jp

OPEN ACCESS

Citation: Kurata K, Shimada K, Takamatsu H (2022) Application of the Taguchi method to explore a robust condition of tumor-treating field treatment. PLoS ONE 17(1): e0262133. https://doi.org/10.1371/journal.pone.0262133

Editor: Maria Grazia Giansanti, Consiglio Nazionale delle Ricerche, ITALY

Received: June 11, 2021

Accepted: December 16, 2021

Published: January 21, 2022

Data Availability Statement: All relevant data are within the paper and its Supporting Information files.

Funding: This study was supported by JSPS KAKENHI Grant Number 18H03520. The funders had no role in study design, data collection and analysis, decision to publish, or preparation of the manuscript.

Competing interests: The authors have declared that no competing interests exist.

Abstract

Tumor-treating fields have potential as minimally invasive cancer treatment. This study aimed to explore the optimum tumor-treating field conditions that minimize unpredicted variations in therapeutic outcomes resulting from differences in cell size and electrical properties. The electric field concentration that induces a dielectrophoretic force near the division plane of a mitotic cell was calculated by finite element analysis for 144 cases, based on different combinations of six noise factors associated with cells and four controllable factors including frequency, as determined by the Taguchi method. Changing the frequency from 200 to 400 kHz strongly increased robustness in producing a dielectrophoretic force, irrespective of noise factors. However, this frequency change reduced the force magnitude, which can be increased by simply applying a higher voltage. Based on additional simulations that considered this trade-off effect, a frequency of 300 kHz is recommended for a robust TTF treatment with allowable variations. The dielectrophoretic force was almost independent of the angle of applied electric field deviated from the most effective direction by ±20 degrees. Furthermore, increased robustness was observed for extracellular fluid with higher conductivity and permittivity. The Taguchi method was useful for identifying robust tumor-treating field therapy conditions from a considerably small number of replicated simulations.

Introduction

A tumor-treating field (TTF) is a weak AC electric field of several hundred kHz to 1 MHz that interferes with cell division. Despite the low intensity of these electric fields, at only a few volts per centimeter, both cell and animal experiments have confirmed that TTFs can arrest tumor cell proliferation and promote cell destruction [1], which renders TTF as a minimally invasive cancer treatment. A pilot clinical trial targeting recurrent glioblastoma (GBM) demonstrated that an AC electric field of 1–2 V/cm at a frequency of 100–200 kHz nearly doubled both the time to disease progression and overall survival (OS) among those reported thus far [2]. A phase III randomized clinical trial for recurrent GBM, which was conducted following these promising preclinical studies, has demonstrated that TTF treatment results are comparable to those for chemotherapy [3]. It has also been reported that TTF is more effective when combined

with chemotherapy [4,5]. Thus, TTF treatment has received the United States Food and Drug Administration (FDA) approval for application to recurrent GBM and newly diagnosed GBM. Following these successes for GBM, numerous trials have been conducted to apply TTF to other cancers in the liver, ovary, lung, and melanoma [6,7]. However, the prognosis for GBM patients is still not satisfactory: the median OS of TTF-treated patients was 14 months, which is only 3 months longer than the OS of those who did not receive TTF treatment [6].

The TTF is considered to impair cell division through several mechanisms. The electric field can modify the alignment of charged molecules, such as tubulin dimers and septin, in a cell. Tubulin dimers are a primary component of microtubules, constituting the spindle for the separation of chromosomes into daughter cells during mitosis. Hence, interference with the tublin dimers due to the force induced by the electric field may disrupt microtubule synthesis and consequently inhibit cell division [8,9]. The electric field also perturbs the localization of septin proteins, which play an important role in protein attachment and barrier formation between mother and daughter cells. Septin dysfunction causes ectopic blebbing and abnormal mitosis [10]. The dielectrophoretic force generated during mitosis may also affect cell division [11]. A dividing cell has an hourglass shape with a cleavage furrow. This shape causes a distortion of the electric field in the cell and results in a concentrated electric field, which generates a dielectrophoretic force on the intracellular polar molecules and thus disrupts normal cell division.

TTF performance is strongly dependent on cell geometry, electrical properties, and the applied electric field. This dependence has been assessed by magnitudes of local intracellular electric fields and dielectrophoretic forces estimated by numerical simulations with assumed electrical properties. The assumed electrical properties of cells were those measured for yeast [12,13], blood cells [14,15], and oocytes [16]. The extracellular electrical properties were assumed to be the same as those of intracellular fluid, blood serum [17,18], or physiological saline [19]. Previous studies have been conducted for combinations of these electric properties, frequency, cell diameter, and membrane thickness (S1 Table) [20–30]. However, because there are many parameters to consider, most of these studies examined the effect of one parameter under a specific combination of other parameters. Therefore, the results highlighted the effects of a major parameter but not the interactions among multiple parameters.

To identify an optimum condition for robust TTF treatment that is not affected by cell geometry or electrical properties, simulations must be conducted for all combinations of parameters for at least six electrical properties: the electrical conductivity and relative permittivity of the intracellular and extracellular fluids and the cell membrane. Such an approach is not realistic because in order to examine three levels for each parameter, for example, simulations must be replicated for 729 (= 3^6) cases. The number of combinations to be considered can be reduced if we design the analyses using the experimental design method established by R. A. Fisher [31] or, even better, the Taguchi method [32], which is a robust design method originally developed to improve the quality of a product. This method has been recently applied to problems in engineering, biotechnology [33–38], and biomedicine [39–42]. The aim of this study is to investigate an optimum setting for robust TTF therapy. To this end, we performed electrical simulations for a mitotic cell model and conducted an analysis using the Taguchi method to identify a condition that generates a suitable local intracellular electric field and dielectrophoretic force, irrespective of uncontrollable variations in cell geometry and electrical properties.

Numerical analysis

We assume a mitotic cell as a target. A three-dimensional cell model was created by overlapping a pair of spherical cells of diameter d with a cell membrane thickness of δ_m and a center-

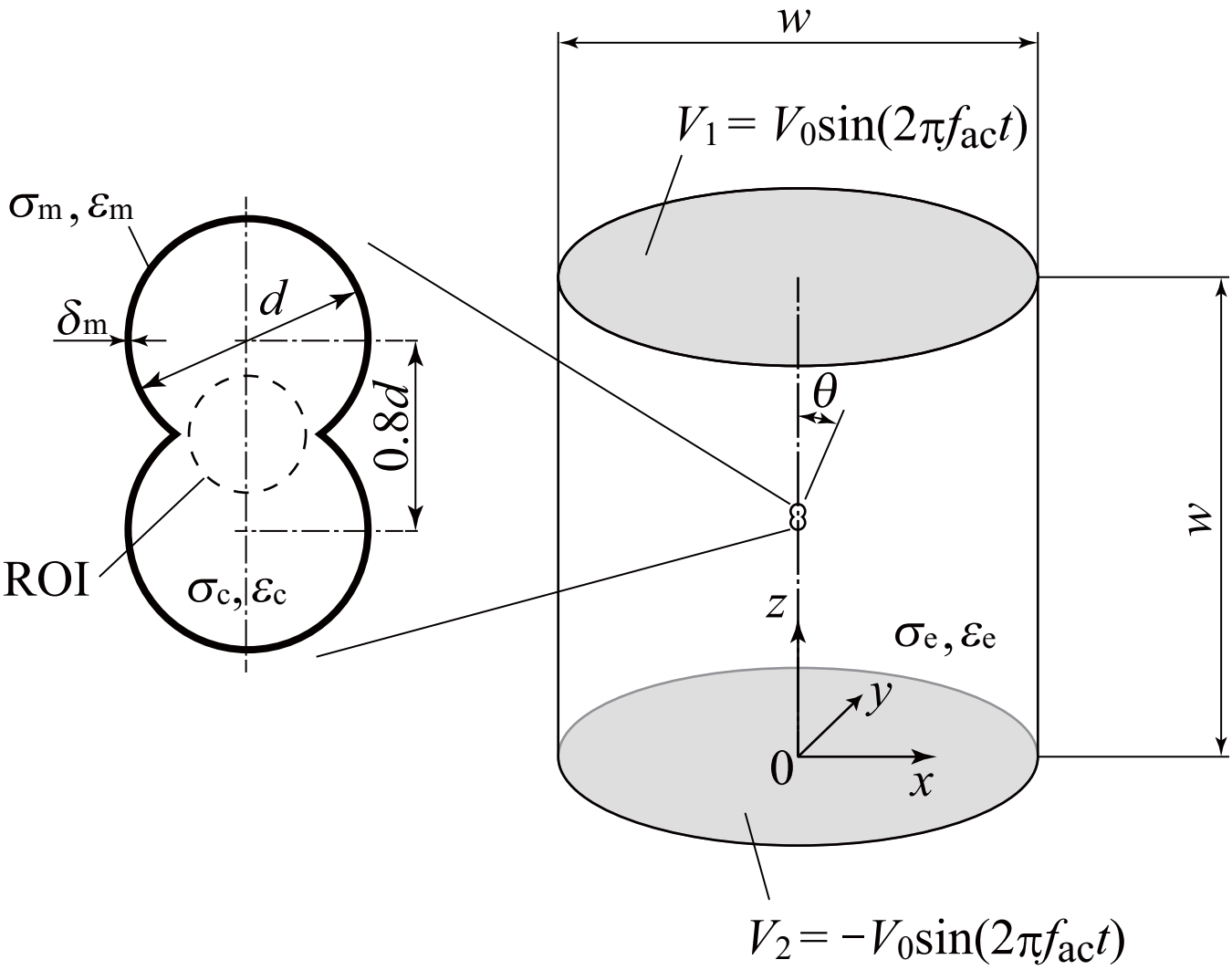

Fig 1. Physical model and coordinate system for calculating the electric field.

https://doi.org/10.1371/journal.pone.0262133.g001

to-center distance of 0.8*d* (Fig 1). To simulate the situation in which the cell is placed in a one-dimensional electric field, we consider a cell in the center of a cylindrical analysis domain that has the same diameter and height *w*, which is sufficiently larger than the cell. The electrical conductivities of the intracellular cytoplasm, cell membrane, and extracellular medium are σ_c, σ_m, σ_e, respectively, and the relative permittivities are ε_c, ε_m, and ε_e, respectively. AC potentials described by

$$V_1 = V_0 \sin(2\pi f_{ac} t) \tag{1}$$

$$V_2 = -V_0 \sin(2\pi f_{ac} t) \tag{2}$$

are applied to the top and bottom of the analysis domain, respectively, where V_0 is the maximum voltage, f_{ac} is the frequency, and t is time. The side of the analysis region is treated as electrically insulated.

We consider the charge conservation law:

$$\nabla J + \partial\rho/\partial t = 0 \tag{3}$$

where J and ρ are the electric current density and charge density, respectively, which are expressed by Ohm's law and Maxwell's equation:

$$J = \sigma E \tag{4}$$

$$\rho = \nabla \cdot (\boldsymbol{\varepsilon}_0 \boldsymbol{\varepsilon} E) \tag{5}$$

Herein, $\boldsymbol{\varepsilon}_0$ is the relative permittivity in a vacuum, and E is the electric field, defined by the gradient of electric potential V:

$$E = -\nabla V \tag{6}$$

By solving these equations via the finite element method, we can determine the distribution of the electric potential and electric field.

If we consider a particle of radius r_p, electrical conductivity σ_p, and relative permittivity $\boldsymbol{\varepsilon}_p$, the dielectrophoretic force F_{dp} acting on the particle is calculated from [43,44]:

$$F_{dp} = 2\pi r_p^3 \boldsymbol{\varepsilon}_0 \boldsymbol{\varepsilon}_c \mathrm{Re}\left(\frac{\boldsymbol{\varepsilon}_p^* - \boldsymbol{\varepsilon}_m^*}{\boldsymbol{\varepsilon}_p^* + 2\boldsymbol{\varepsilon}_m^*}\right) \nabla (E_{rms})^2 \tag{7}$$

where E_{rms} $(= E/\sqrt{2})$ is the effective electric field and Re indicates the real part of a complex number given in terms of

$$\boldsymbol{\varepsilon}_p^* = \boldsymbol{\varepsilon}_p - i\sigma_p/(2\pi f_{ac}) \tag{8}$$

$$\boldsymbol{\varepsilon}_m^* = \boldsymbol{\varepsilon}_m - i\sigma_m/(2\pi f_{ac}) \tag{9}$$

with i as the imaginary unit. The term $2\pi r_p^3 \boldsymbol{\varepsilon}_0 \boldsymbol{\varepsilon}_c \mathrm{Re}\left(\frac{\boldsymbol{\varepsilon}_p^* - \boldsymbol{\varepsilon}_m^*}{\boldsymbol{\varepsilon}_p^* + 2\boldsymbol{\varepsilon}_m^*}\right)$ in (7) is almost constant for a tubulin dimer, a main target of TTF, for an AC electric field on the order of several hundred kilohertz. Thus,

$$|F_{dp}| \propto |\nabla (E_{rms})^2| \tag{10}$$

Therefore, we will focus on $\nabla(E_{rms})^2$ to evaluate the magnitude of the dielectrophoretic force.

Finite element analysis was conducted using COMSOL Multiphysics software (v. 5.3a, COMSOL AB, Stockholm, Sweden) equipped with an AC/DC module. Assuming w = 20 mm, the cylindrical analysis domain was divided into approximately 180 million tetrahedral elements. Based on previous studies that indicated a successful TTF treatment using intracellular electric fields ranging from 1 to 3 V/cm, we conducted simulations for V_0 = 1, 2, 3, and 4 V, which generate external electric fields of 1, 2, 3, and 4 V/cm, respectively. The simulations were based on various combinations of frequency, cell size, and electrical properties, as summarized in Tables 1 and 2. The effect of a cell membrane that is extremely thin compared with the cell size was considered by applying the contact impedance boundary condition available in COMSOL.

Fig 2 shows examples of the distribution of the effective electric field E_{rms} and the gradient of the square of the effective electric field $\nabla(E_{rms})^2$, which were obtained for V_0 = 1 V using the parameters classified as level 2 in Table 1. Five pairs of results correspond to combinations of six other parameters (noise factors described in the next section) grouped by analysis

Table 1. Controllable factors and levels examined by the Taguchi method.

Controllable factor	Parameters	Level 1	Level 2	Level 3
C_1	Frequency, f_{ac} (kHz)	100	200	400
C_2	Direction of cell division, θ (deg)	10	0	20
C_3	Electrical conductivity of the extracellular medium, σ_e (S/m)	0.3	1.2	3
C_4	Relative permittivity of the extracellular medium, ε_e (-)	60	72.3	80

https://doi.org/10.1371/journal.pone.0262133.t001

Table 2. Noise factors and levels examined by the Taguchi method.

Noise factor	Parameters	Level 1	Level 2	Level 3
N_1	Thickness of the cell membrane, δ_m (nm)	3	5	7
N_2	Cell diameter, d (μm)	10	20	100
N_3	Electrical conductivity of the cytoplasm, σ_c (S/m)	0.1	0.3	1
N_4	Relative permittivity of the cytoplasm, ε_c (-)	60	72.3	80
N_5	Electrical conductivity of the cell membrane, σ_m (S/m)	1×10^{-8}	3×10^{-7}	1×10^{-6}
N_6	Relative permittivity of the cell membrane, ε_m (-)	2.5	5	10

https://doi.org/10.1371/journal.pone.0262133.t002

number from No. 1 to No. 5 in Table 3. For case No. 1 to No. 4, a concentration of the electric field was observed at the cleavage furrow of the cell. This concentration resulted in an extremely high $\nabla(E_{rms})^2$ at the neck. In contrast, no increase or concentration of the electric field or $\nabla(E_{rms})^2$ was observed for No. 5. These results indicate that the distribution of

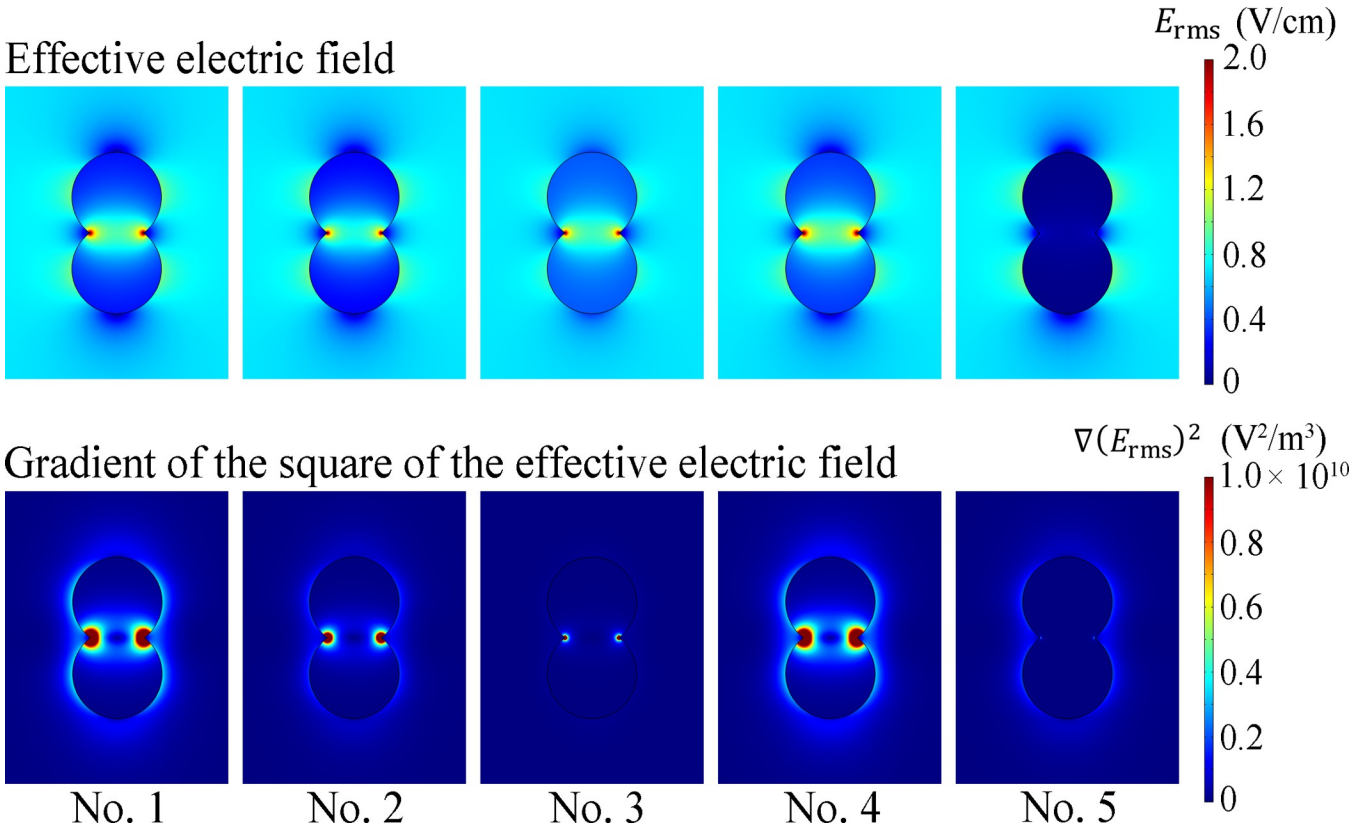

Fig 2. Distribution of the effective electric field E_{rms} (top) and the gradient of the square of the effective electric field $\nabla(E_{rms})^2$ (bottom) for V_0 = 1 V, obtained using the parameters classified as level 2 in Table 2 with the other parameters grouped by analysis number from No. 1 to No. 5 in Table 3.

https://doi.org/10.1371/journal.pone.0262133.g002

Table 3. Layout of L18 orthogonal array for noise compounding.

	Noise factor										δ_m (nm)	d (μm)	σ_c (S/m)	ε_c (-)	σ_m (S/m)	ε_m (-)
Anal. No.	N_A	N_B	N_1	N_2	N_3	N_4	N_5	N_6	N_A	N_B	N_1	N_2	N_3	N_4	N_5	N_6
1	1	1	1	1	1	1	1	1	N/A	N/A	3	10	0.1	60	1×10^{-8}	2.5
2	1	1	2	2	2	2	2	2	N/A	N/A	5	20	0.3	72.3	3×10^{-7}	5
3	1	1	3	3	3	3	3	3	N/A	N/A	7	100	1	80	1×10^{-6}	10
4	1	2	1	1	2	2	3	3	N/A	N/A	3	10	0.3	72.3	1×10^{-6}	10
5	1	2	2	2	3	3	1	1	N/A	N/A	5	20	1	80	1×10^{-8}	2.5
6	1	2	3	3	1	1	2	2	N/A	N/A	7	100	0.1	60	3×10^{-7}	5
7	1	3	1	2	1	3	2	3	N/A	N/A	3	20	0.1	80	3×10^{-7}	10
8	1	3	2	3	2	1	3	1	N/A	N/A	5	100	0.3	60	1×10^{-6}	2.5
9	1	3	3	1	3	2	1	2	N/A	N/A	7	10	1	72.3	1×10^{-8}	5
10	2	1	1	3	3	2	2	1	N/A	N/A	3	100	1	72.3	3×10^{-7}	2.5
11	2	1	2	1	1	3	3	2	N/A	N/A	5	10	0.1	80	1×10^{-6}	5
12	2	1	3	2	2	1	1	3	N/A	N/A	7	20	0.3	60	1×10^{-8}	10
13	2	2	1	2	3	1	3	2	N/A	N/A	3	20	1	60	1×10^{-6}	5
14	2	2	2	3	1	2	1	3	N/A	N/A	5	100	0.1	72.3	1×10^{-8}	10
15	2	2	3	1	2	3	2	1	N/A	N/A	7	10	0.3	80	3×10^{-7}	2.5
16	2	3	1	3	2	3	1	2	N/A	N/A	3	100	0.3	80	1×10^{-8}	5
17	2	3	2	1	3	1	2	3	N/A	N/A	5	10	1	60	3×10^{-7}	10
18	2	3	3	2	1	2	3	1	N/A	N/A	7	20	0.1	72.3	1×10^{-6}	2.5

N_A and N_B denote blank columns with no noise factors assigned.

https://doi.org/10.1371/journal.pone.0262133.t003

$\nabla(E_{rms})^2$ and thus the dielectrophoretic force strongly depend on the electrical properties. Because the results demonstrated that an applied voltage caused the electric field to be concentrated near the cleavage furrow, we defined a spherical region in the center shown in Fig 1 as the region of interest (ROI) and calculated the mean value of $\nabla(E_{rms})^2$. The diameter of the ROI was determined as 80% of the length at the furrow.

Taguchi method

Among numerous factors that influence the outcome, those that are controlled by operation are separated from uncontrollable factors that are unknown or that exhibit variations. The Taguchi method was introduced to examine the influence of the controllable factors that display a more robust effect on the outcome irrespective of the uncontrollable factors, which are considered as noise. To this end, the output of interest, $\nabla(E_{rms})^2$ in the ROI, was evaluated for combinations of the controllable factors and noise factors. The signal-to-noise (S/N) ratio, defined as the variation in output with respect to noise, is an important measure for judging the robustness of the influence of controllable factors. Therefore, we sought to identify a combination of controllable factors that maximizes the S/N ratio in order to determine the optimum operation condition that minimizes the effect of noise.

Parameter diagram of the TTF system

The Taguchi method addresses the optimization of a problem that has a linear relationship between an input M and an output y, i.e., $y = \beta M$, where M is the external electric field in the present study. Based on our preliminary analysis, which confirmed this linear relationship, the square root of the mean $\nabla(E_{rms})^2$ in the ROI is taken as y. The proportional constant β is determined from simulations conducted for four levels of the input, M = 1, 2, 3, and 4 V/cm, and was utilized to evaluate the significance of the electric field.

Four factors, i.e., the frequency of the electric field, the electric field direction with respect to the cell, and the electrical conductivity and relative permittivity of the extracellular medium, were selected as controllable factors (respectively denoted by C_i (i = 1–4) in Table 1). The frequency is a major factor that is selected in TTF treatment. The direction of cell division with respect to the external electric field is expected to strongly influence the treatment outcome because the electric field concentration at the neck of the cell division plane is most effective for generating a dielectrophoretic force. Although the relative direction cannot be controlled in treatment owing to the unpredictable and varying directions of cell division, it is considered as a controllable factor to clarify its effect. Similarly, although the electrical conductivity and relative permittivity of the extracellular fluid are not easily controlled, these parameters are included as controllable factors in order to examine the efficacy of administrating exogenous solutions, such as imaging contrast agents, to modify electrical properties.

The remaining factors that significantly influence the outcome but are uncontrollable are selected as noise factors (denoted as N_i (i = 1–6) in Table 2). These factors include the cell membrane thickness, cell diameter, and electrical conductivities and relative permittivities of the cytoplasm and cell membrane. The cell membrane thickness and cell diameter are inherently variable and unpredictable. The electrical properties of the intracellular fluid and cell membrane are also uncontrollable and strongly depend on cell type (S1 Table).

The problem addressed in this work is summarized in Fig 3 as a parameter diagram (P-diagram) that indicates the relationship among the input, output, control factors, and noise factors of the TTF system. The values of the control factors and noise factors, selected for each of three levels, are summarized in Tables 1 and 2. These values were determined based on the parameter ranges shown in S1 Table. The frequency used in current TTF therapeutic devices, the electric field direction considered to maximize the dielectrophoretic force, and the electrical conductivity and relative permittivity values most commonly used in previous studies, i.e., f_{ac} = 200 kHz, θ = 0, σ_e = 1.2 S/m, and ε_e = 72.3, were assigned to level 2, and the combination of level 2 values was denoted as a reference set of controllable factors, C_{ref}.

Noise compounding

Combinations of the levels of each noise factor used in the analysis are shown in Table 3. Eighteen combinations were selected from an L18 orthogonal array such that the noise factor of each level encountters six times. Using level 2 values for all controllable factors from C_1 to C_4, we conducted numerical analyses for 18 combinations of noise factors for four levels of input M to determine $\sqrt{|\nabla(E_{rms})^2|}$ in the ROI as the output, y. The effects of noise factors on β and the S/N ratio were evaluated as follows (S2 Table).

The value of β is determined by

$$\beta = \sum My/r \tag{11}$$

where

$$\sum My = \sum_{i=1}^{4} M_i y_i \tag{12}$$

$$r = \sum_{i=1}^{4} M_i^2 \tag{13}$$

The S/N ratio is defined by

$$\mathrm{S/N} = 10\log(\beta^2/V_{Noise}) \tag{14}$$

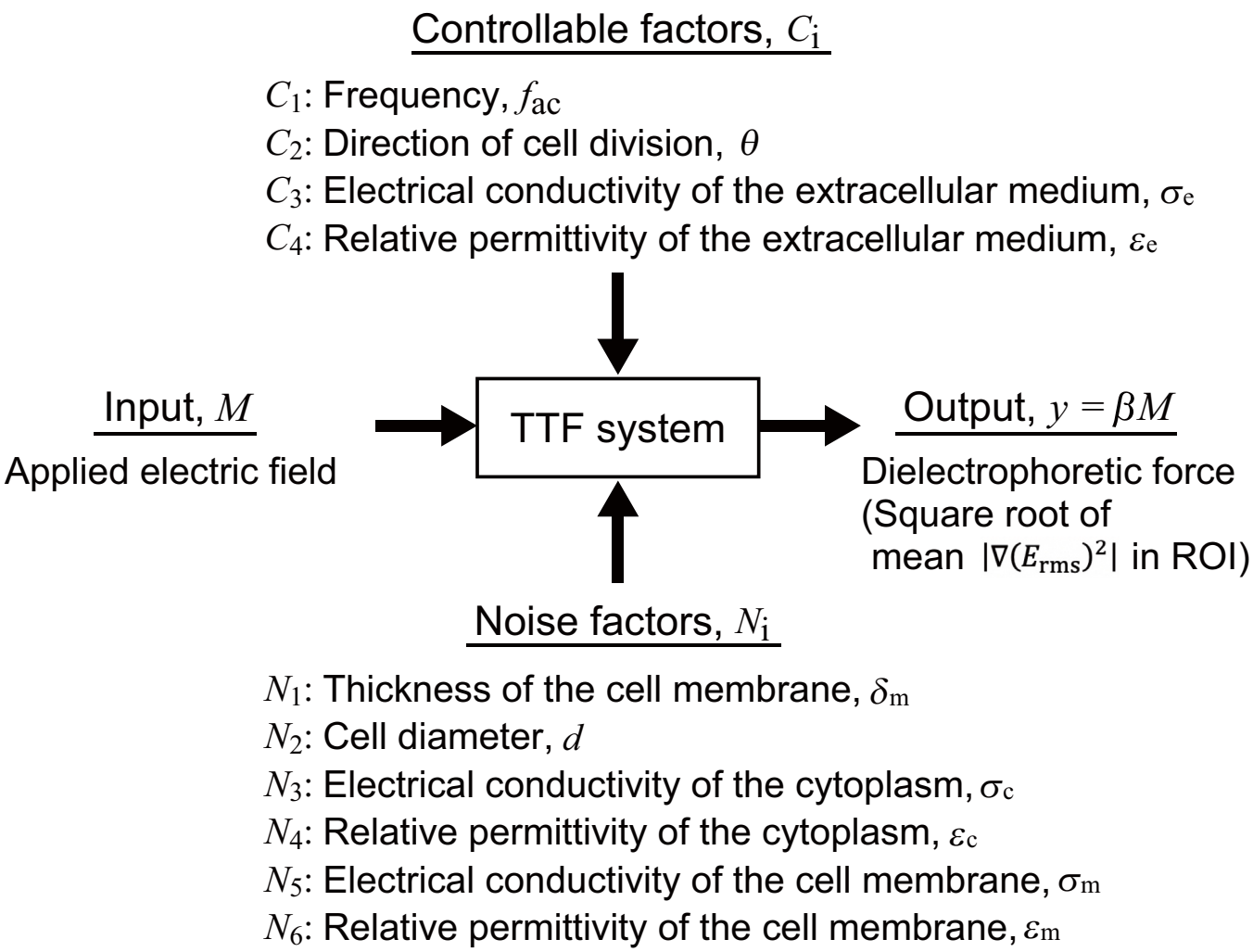

Fig 3. Parameter diagram of the TTF system.

https://doi.org/10.1371/journal.pone.0262133.g003

where the noise variance, V_{Noise}, is determined from

$$V_{Noise} = S_{Noise}/(n-1) \tag{15}$$

based on the following values:

$$S_T = \sum_{i=1}^{4} y_i^2 \tag{16}$$

$$S_\beta = (\sum My)^2/r \tag{17}$$

$$S_{Noise} = S_T - S_\beta \tag{18}$$

The value of β obtained by averaging that of six data sets for each noise factor, which is denoted by N_{ij} for level j of noise factor N_i, is shown in Fig 4. Although β is lower for higher levels of N_1, N_2, N_3, and N_4, the value for N_5 was the lowest for level 2. The level of N_6 had little

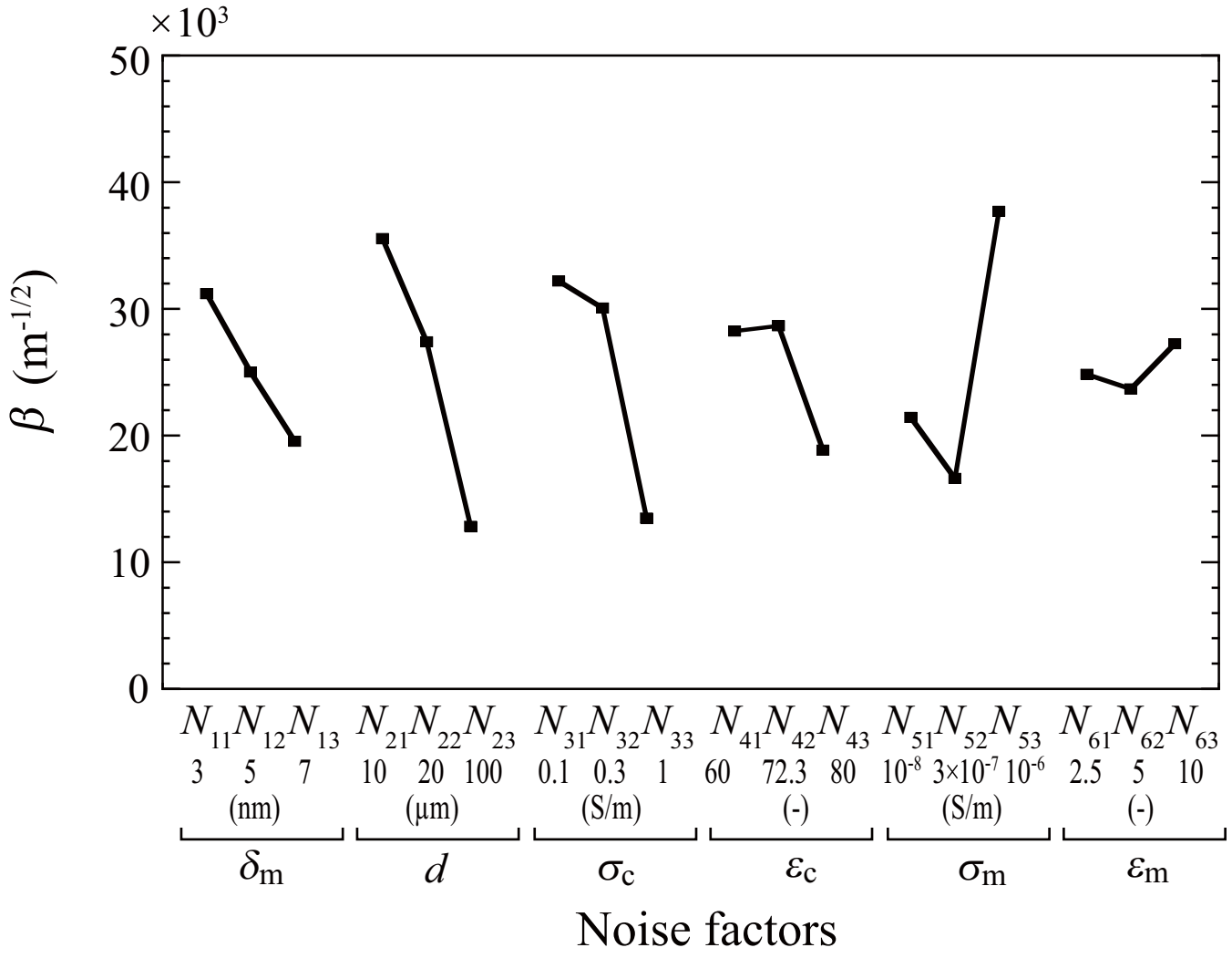

Fig 4. Effect of each noise factor on the mean value of β. N_{ij} denotes the effect of level j for factor i.

https://doi.org/10.1371/journal.pone.0262133.g004

effect on β. The results shown in Fig 4 indicate that the combination of levels with the highest β was N_{11}–N_{21}–N_{31}–N_{41}–N_{53}–N_{63} whereas the combination with the lowest β was N_{13}–N_{23}–N_{33}–N_{43}–N_{52}–N_{62}. Here, we denote these sets of compounded noise factors as N_{max} and N_{min}, respectively, as summarized in Table 4.

Table 4. Combination of noise factors that minimized (N_{min}) and maximized (N_{max}) β obtained by noise compounding.

	Compounded noises			
Noise factor	N_{min}		N_{max}	
Thickness of the cell membrane, δ_m (nm)	N_{13}	7	N_{11}	3
Cell diameter, d (μm)	N_{23}	100	N_{21}	10
Electrical conductivity of the cytoplasm, σ_c (S/m)	N_{33}	1	N_{31}	0.1
Relative permittivity of the cytoplasm, ε_c (-)	N_{43}	80	N_{41}	60
Electrical conductivity of the cell membrane, σ_m (S/m)	N_{52}	3×10^{-7}	N_{53}	1×10^{-6}
Relative permittivity of the cell membrane, ε_m (-)	N_{62}	5	N_{63}	10

https://doi.org/10.1371/journal.pone.0262133.t004

Factorial effects of control factors

Next, with the set of noise factors fixed at N_{max} and N_{min}, finite element analyses were conducted for 18 combinations of four controllable factors selected from the L18 orthogonal array, which includes six cases of the same level for each controllable factor (S3 Table). Again, the analyses were performed for four levels of input M. The values of β and the S/N ratio were determined by Eqs (11) and (14), respectively.

Fig 5 shows the effect of controllable factors on β and the S/N ratio, with each given as the average of six data sets for each controllable factor C_{ij}, the level j of factor C_i. The influence of factor C_1 (frequency) on both the S/N ratio and β was much greater than that of the other factors. Although the average value of β was the largest for level 1 (C_{11}), the S/N ratio was extremely small, suggesting that the output was easily influenced by noise. Therefore, an increased input (applied electric field) did not always result in a considerable increase in the output. In contrast, C_{13} showed a very high S/N ratio and a moderate β, indicating a solid effect irrespective of the combinations of other factors. Therefore, a robust effect is expected for C_{13}, level 3 of C_1. For the same reason, the condition that resulted in the highest S/N ratio for each factor is preferable. Thus, we obtained the combination C_{13}–C_{21}–C_{33}–C_{43} as an optimum set of controllable factors, C_{opt}.

The increase in the output y ($\sqrt{|\nabla(E_{\mathrm{rms}})^2|}$ in the ROI) with the input M (applied electric field) for the above-determined conditions is shown in Fig 6. The output increased almost linearly under all conditions, satisfying the requirement of the Taguchi method. The values of y obtained for level 2 of all controllable factors, C_{ref}, with the set of noise factors N_{min} was the lowest, whereas that with N_{max} was the highest, being more than two-fold higher than the former result. Hence, the result obtained for the other combinations of noise factors with C_{ref} will fall between these two lines. In contrast, the result for the set of control factors C_{opt} and N_{max} was similar to that for C_{opt} and N_{min}, with a difference of 3%. This finding suggests that the result for the set of controllable factors C_{opt} was almost independent of noise factors, indicating that the output was robust.

Validation and tuning

Although β was not influenced by noise factors for the set of controllable factors C_{opt}, β was much smaller than the highest value obtained for C_{ref} and N_{max}. Therefore, the final goal of the analysis is to find the optimum condition, i.e., a combination of controllable factors that results in a higher β with an allowable S/N ratio.

First, finite element analysis was conducted for four combinations of controllable factors and noise factors, C_{opt} (C_{13}–C_{21}–C_{33}–C_{43})–N_{min}, C_{opt}–N_{max}, C_{ref} (C_{12}–C_{22}–C_{32}–C_{42})–N_{min}, and C_{ref}–N_{max} with inputs of M = 1, 2, 3, and 4 V/cm. To determine whether the results could be predicted from the data that had already been obtained, the S/N ratio, η_{opt}, η_{ref}, and the values of β, β_{opt}, and β_{ref} were predicted from the following equations:

$$\eta_{\mathrm{opt}} = \eta_{\mathrm{T}} + (\eta_{C13} - \eta_{\mathrm{T}}) + (\eta_{C21} - \eta_{\mathrm{T}}) + (\eta_{C33} - \eta_{\mathrm{T}}) + (\eta_{C43} - \eta_{\mathrm{T}}) \tag{19}$$

$$\eta_{ref} = \eta_{\mathrm{T}} + (\eta_{C12} - \eta_{\mathrm{T}}) + (\eta_{C22} - \eta_{\mathrm{T}}) + (\eta_{C32} - \eta_{\mathrm{T}}) + (\eta_{C42} - \eta_{\mathrm{T}}) \tag{20}$$

$$\beta_{\mathrm{opt}} = \beta_{\mathrm{T}} + (\beta_{C13} - \beta_{\mathrm{T}}) + (\beta_{C21} - \beta_{\mathrm{T}}) + (\beta_{C33} - \beta_{\mathrm{T}}) + (\beta_{C43} - \beta_{\mathrm{T}}) \tag{21}$$

$$\beta_{ref} = \beta_{\mathrm{T}} + (\beta_{C12} - \beta_{\mathrm{T}}) + (\beta_{C22} - \beta_{\mathrm{T}}) + (\beta_{C32} - \beta_{\mathrm{T}}) + (\beta_{C42} - \beta_{\mathrm{T}}) \tag{22}$$

where η_{Cij} and β_{Cij} are the values for level j of controllable factor i, respectively, and η_{T} and β_{T} are the average of all data.

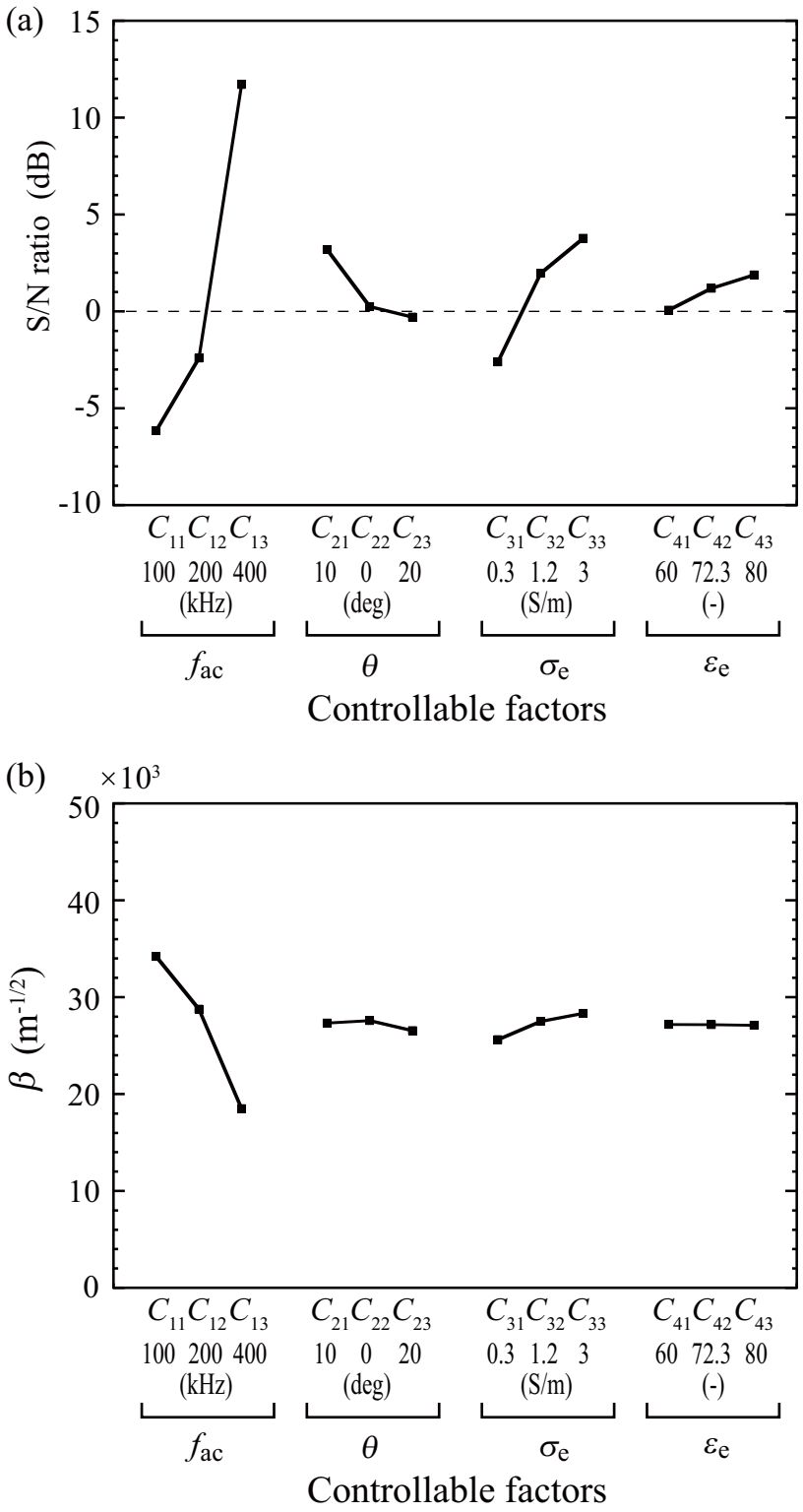

Fig 5. Effect of each controllable factor on the mean of the S/N ratio (a) and β (b). C_{ij} denotes the effect of level j for factor i.

https://doi.org/10.1371/journal.pone.0262133.g005

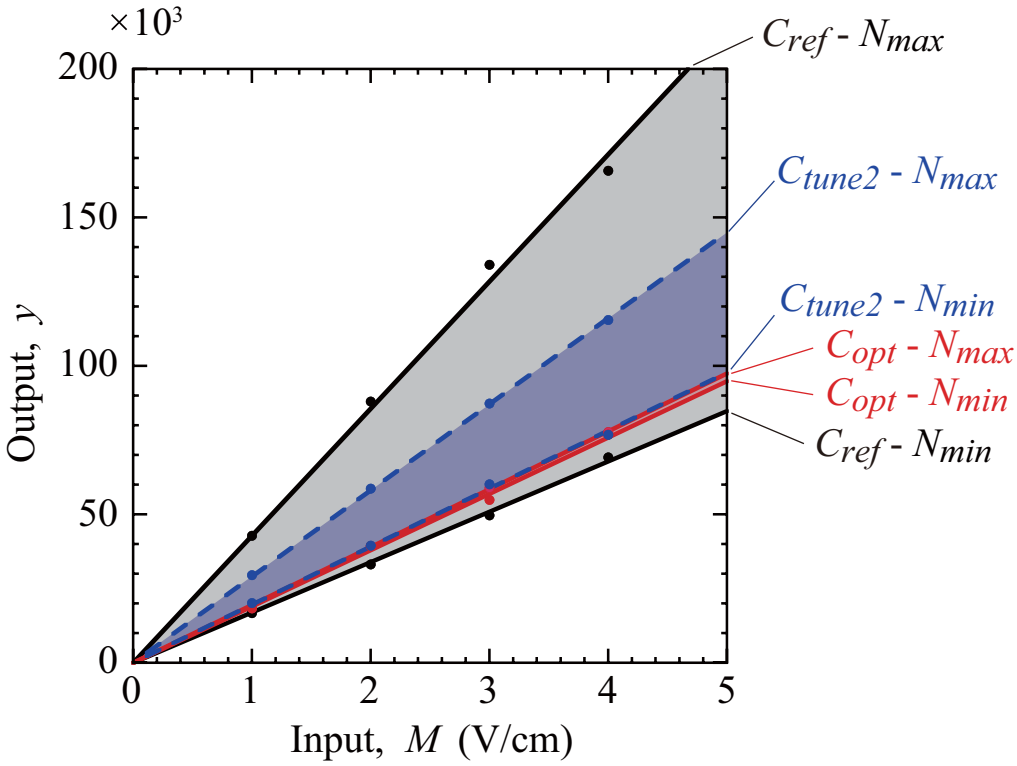

Fig 6. Relationship between the input M (applied electric field) and the output y (square root of $\nabla(E_{rms})^2$).

https://doi.org/10.1371/journal.pone.0262133.g006

The results are listed in Table 5. The numerical simulation showed that as the parameters changed from C_{ref} to C_{opt}, the S/N ratio increased by 25.2 dB, whereas β decreased from 29.9×10^3 $m^{-1/2}$ to 19.2×10^3 $m^{-1/2}$. This trend indicates that although β decreased by 36%, the output fluctuation decreased considerably to 5.5% of that for C_{ref}. The percentage variation relative to the compared condition, P (%), corresponding to an S/N ratio increase of x dB (gain Δ) is

$$P = 0.5^{\frac{x}{6}} \times 100 \tag{23}$$

Table 5. Comparison of the S/N ratio and β obtained for different sets of parameters.

		S/N ratio, η (dB)			
Combination		Predicted	Gain Δ η-η_{ref}	Validated	Gain Δ η-η_{ref}
C_{ref}	C_{12}-C_{22}-C_{32}-C_{42}	-2.1		-2.1	
C_{opt}	C_{13}-C_{21}-C_{33}-C_{43}	17.4	19.6	23.1	25.2
C_{tune1}	C_{12}-C_{21}-C_{33}-C_{43}	3.3	5.4	-1.8	0.2
C_{tune2}	300kHz-C_{21}-C_{33}-C_{43}	N/A	N/A	4.9	6.9

		β ($m^{-1/2}$)					
Combination		Predicted		β/β_{ref}	Validated		β/β_{ref}
C_{ref}	C_{12}-C_{22}-C_{32}-C_{42}	29.6	$\times10^3$		29.9	$\times10^3$	
C_{opt}	C_{13}-C_{21}-C_{33}-C_{43}	19.8		0.67	19.2		0.64
C_{tune1}	C_{12}-C_{21}-C_{33}-C_{43}	30.1		1.02	31.2		1.04
C_{tune2}	300kHz-C_{21}-C_{33}-C_{43}	N/A		N/A	24.3		0.81

https://doi.org/10.1371/journal.pone.0262133.t005

The increase in the S/N ratio of the predicted result was relatively smaller, 19.6 dB, corresponding to a variation reduction to 10.4% of that for C_{ref}. However, the other values, including β for C_{ref} and C_{opt} and the S/N ratio for C_{ref}, agreed well with the numerical simulation, indicating the validity of the Taguchi method.

We found that selecting the combination C_{opt} rather than C_{ref} considerably increases the robustness, with much less influence due to noise factors. However, β was much smaller, suggesting that a higher voltage is needed to induce an electric field that can generate an adequate dielectrophoretic force. Although increasing both β and the S/N ratio is not possible because of their trade-off relationship, it is possible to find a condition that results in a higher β with an allowable S/N ratio. Because the frequency has a significant effect on the outcome, 200 kHz (C_{12}) and 300 kHz (not included in Table 1) were examined instead of 400 kHz (C_{13}) in C_{opt} by additional numerical simulations. In the result for 200 kHz, the S/N ratio was much lower than that for C_{opt} and only 0.2 dB higher than that for C_{ref}, even though β was considerably higher (Table 5). In contrast, compared with the result for C_{opt}, the application of 300 kHz increased β by 27% from 19.2×10^3 $m^{-1/2}$ to 24.3×10^3 $m^{-1/2}$ whereas the S/N ratio was maintained at 4.9 dB, which is 18.3 dB lower than that for C_{opt} but 6.9 dB higher than that for C_{ref}.

Discussion

In this study, a robust condition of TTF treatment was identified, with the goal of minimizing the variation in therapeutic outcomes irrespective of differences in cell size and electrical properties. TTF therapy aims to generate a dielectrophoretic force on intracellular molecules by application of an electric field, ultimately interfering with cell division. Based on a linear relationship between the applied electric field (input M) and the square root of the dielectrophoretic force (output y) at the ROI, i.e., $y = \beta M$, we identified a TTF condition that minimizes the variation in β owing to unpredicted variations in unknown cell sizes and electrical properties.

We first selected four controllable factors and six uncontrollable noise factors that influence β. If three levels of each factor are to be examined, the simulation must be replicated 3^{10} (= 59,049) times for all combinations of the selected factors. Therefore, the Taguchi method, which is a powerful tool for optimization problems, was used to reduce the number of replicates by using an orthogonal array of combination factors. The main effect and interaction of each factor were simultaneously evaluated by combining each level of a factor equally with the other factors in the orthogonal array. Considering that the assignment of four controllable factors and six noise factors to the L18 orthogonal array and four levels of applied electric field (input M) still requires a simulation of 1,296 (= 18 × 18 × 4) replicates, the number of simulations was further decreased by compounding noise factors into two combinations that maximize and minimize β, respectively, which were determined before the control factors were examined. By assigning four control factors to the L18 orthogonal array with two combinations of noise factors and four levels of applied electric field, the numerical simulation was replicated for 144 (= 18 × 2 × 4) cases.

The six uncontrollable factors considered as noise were the cell membrane thickness, cell diameter, and electrical conductivities and relative permittivities of the intracellular fluid and cell membrane. The membrane thickness was assumed to be 3–7 nm in this study, and the cell diameter was assumed as 10–100 μm based on previous studies (S1 Table). The assumed range of electrical properties covered those used in most of these previous studies. The electrical properties of the intracellular fluid and cell membrane strongly depend on cell type [45,46], and those measured for cultured cells may differ from those in the human body in an aggregate state. Therefore, finding a reliable condition for a variety of these properties is important for successful TTF therapy.

Table 6. Comparison of the S/N ratio and β obtained for different angles.

		S/N ratio, η (dB)			
Combination		Predicted	Gain $\Delta\ \eta$-η_{ref}	Validated	Gain $\Delta\ \eta$-η_{ref}
C_{ref}	C_{12}-C_{22}-C_{32}-C_{42}	-2.1		-2.1	
C_{opt}	C_{13}-C_{21}-C_{33}-C_{43}	17.4	19.6	23.1	25.2
$C_{20°}$	C_{13}-20˚-C_{33}-C_{43}	13.9	16.0	16.2	18.3
$C_{30°}$	C_{13}-30˚-C_{33}-C_{43}	N/A	N/A	6.1	8.2
$C_{45°}$	C_{13}-45˚-C_{33}-C_{43}	N/A	N/A	0.8	2.9
		β ($m^{-1/2}$)			
Combination		Predicted	β/β_{ref}	Validated	β/β_{ref}
C_{ref}	C_{12}-C_{22}-C_{32}-C_{42}	29.6 $\times 10^3$		29.9 $\times 10^3$	
C_{opt}	C_{13}-C_{21}-C_{33}-C_{43}	19.8	0.67	19.2	0.64
$C_{20°}$	C_{13}-20˚-C_{33}-C_{43}	19.0	0.64	19.9	0.67
$C_{30°}$	C_{13}-30˚-C_{33}-C_{43}	N/A	N/A	20.4	0.68
$C_{45°}$	C_{13}-45˚-C_{33}-C_{43}	N/A	N/A	20.5	0.69

https://doi.org/10.1371/journal.pone.0262133.t006

The frequency of the applied electric field was the first-priority controllable factor, which ranged from 100 to 400 kHz. This range, which is much narrower than that employed in previous studies (a few kHz to several GHz (S1 Table)), was selected based on the finding that several hundred kHz is the most effective frequency for inhibiting cell proliferation [11,28]. Actually, frequencies of 200 and 150 kHz are used in the Optune system (Novocure Ltd.) and Novo TTF-100L, respectively, which are commercially available TTF therapeutic devices. We found that a lower frequency can potentially increase the dielectrophoretic force. However, this trend largely depends on other factors, indicating a considerably lower S/N ratio at lower frequencies (Fig 5). This trade-off effect of frequency on the dielectrophoretic force and the S/N ratio is one of the most important findings in this study.

The second controllable factor, the direction of the applied electric field with respect to the plane of cell division, cannot be controlled in clinical TTF therapy owing to the unknown, unpredictable direction of cell division in the human body. It is obvious that the largest dielectrophoretic force is produced when the electric field is applied perpendicular to the division plane, because the dielectrophoretic force is a result of electric field distortion near the cleavage furrow. However, the direction was considered as a controllable factor to clarify how the dielectrophoretic force decreases as the direction deviates from the desired angle. The results indicate that the dielectrophoretic force is nearly independent of the angle within a range of ±20 degrees, showing a variation of less than 4 dB (Fig 5). This finding suggests that using five pairs of electrodes placed at angles of 36 degrees each around a target tissue will produce an adequate dielectrophoretic force in the cells, independent of the direction of cell division. To further investigate the effect of the direction of the electric field on the robustness of TTF, additional analysis was conducted, in which the angles shifted to 20˚, 30˚, and 45˚ were assigned to the L18 orthogonal array. The S/N ratio and β obtained from this analysis are shown in Table 6. Even if the angle was changed from the most robust condition of C_{opt} to 20˚ ($C_{20°}$), the S/N ratio was still 18.3 dB higher than that for C_{ref}. This indicates that the output fluctuation decreased to 12.1% of that for C_{ref}. As the angle was further changed to 30˚ ($C_{30°}$) and 45˚ ($C_{45°}$), the improvement in robustness was decreased to 8.2 dB and 2.9 dB, which resulted in the output fluctuation being reduced to only 38.8% and 72.5% of C_{ref}, respectively. On the other hand, the effect of the angle on β was negligible; β decreased irrespective of the angle, and was approximately 0.7 times as small as that for C_{ref}.

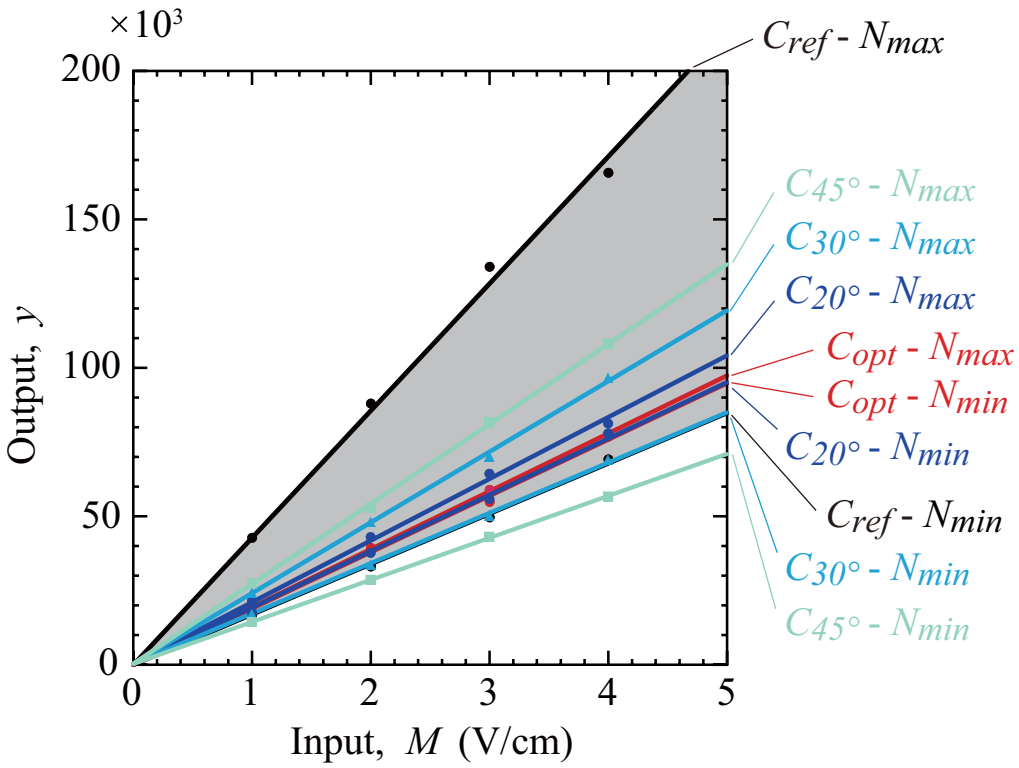

Fig 7. Relationship between the input *M* (applied electric field) and the output *y* (square root of $\nabla(E_{rms})^2$) obtained for different angles.

https://doi.org/10.1371/journal.pone.0262133.g007

TTF efficacy is maximal when the axis of cell division is parallel to the electric field [1,2]. Therefore, in clinical applications, TTF is commonly delivered to a target tumor by using multiple pairs of electrodes because cells undergo mitosis in different spatial orientations [47,48]. The analysis for $\theta = 20^\circ$, 30°, and 45° corresponds to the treatment using five pairs, three pairs, and two pairs of electrodes, respectively (S1 Fig). Increasing the number of electrode pairs from two to three and five improved the robustness by 5.3 dB (= 6.1–0.8 dB) and 15.4 dB (= 16.2–0.8 dB), respectively, which indicates that the output fluctuation decreased to 54.2% and 16.9%. Fig 7 shows the increase in the output y with the input M for angles of 20°, 30°, and 45°. The result for C_{20° ($\theta = 20^\circ$) and noise factors N_{max} was only 9.4% different from that for the set of C_{20° and N_{min}. The difference caused by uncontrollable noises increased to 41% for C_{30° ($\theta = 30^\circ$) and 90% for C_{45° ($\theta = 45^\circ$). This indicates that TTF treatment using two orthogonal sets of electrodes is much more susceptible to noise factors than that using five sets of electrodes. However, there are limitations to this finding; electrodes on a single plane may not be sufficient to obtain the expected effect because cells will divide in all directions three-dimensionally while being exposed to non-uniform electric fields depending on the location. Furthermore, the feasibility of a multiple-electrode setup would be an issue for clinical applications. In order to take the complex anatomy and unknown direction of cell division into account, it is essential to combine a MR image-based finite element model of tumors with a realistic electrode layout, as previously reported by Korshoej et al. [49–51].

The electrical properties of the extracellular fluid, i.e., the third and fourth controllable factors, are inherently uncontrollable, but were included as controllable factors to examine the feasibility of changing these properties by injecting an exogenous solution. A higher

extracellular conductivity increased the robustness of the TTF treatment (Fig 5(A)) and slightly increased the dielectrophoretic force (Fig 5(B)). This increased conductivity can be achieved by injecting saline (1.4 S/m), which has a conductivity slightly higher than that of blood serum (1.2 S/m), considered as level 2 in this study. However, other solutions such as angiographic agents should not be used because of their lower electric conductivity: 0.5 S/m for Gd-based electrolytic contrast agents of magnetic resonance imaging (MRI), such as Magnevist and Dotarem, and 0.01 S/m for a non-electrolytic Fe-based agent, EM1301 [52]. Therefore, the administration of exogenous agents is not desirable for enhancing the TTF effect. More importantly, it should be noted that the MRI contrast agent used for imaging may have a negative effect on the robustness of the treatment if the agent remains in the target area. Increasing another factor, the dielectric effect, also slightly increased the S/N ratio. However, in this respect, no liquid seems to be superior to water, which has a high relative permittivity of 80.

In agreement with a previous study [28], we found that the dielectrophoretic force was significantly smaller in larger cells (Fig 4). A previous study reported unintended cell expansion during TTF treatment [53]. Therefore, it is plausible that repeated TTF therapy will become less effective for cells that become larger due to TTF *per se*.

In this work, the most important indicator for the optimization problem is the S/N ratio, which represents the robustness of the outcome. Even when the output β is high on average, it does not mean that the application of a higher voltage always produces large dielectrophoretic forces in cells if the S/N ratio is considerably low. Meanwhile, if the S/N ratio is relatively high, we can induce larger dielectrophoretic forces by applying a higher voltage only if β is positive. From this viewpoint, the optimum condition C_{opt} (C_{13}–C_{21}–C_{33}–C_{43}) was considerably better than C_{ref} (C_{12}–C_{22}–C_{32}–C_{42}) because the S/N ratio was higher by 25.2 dB (Table 5), corresponding to a reduced variation in the output, which decreased to one eighteenth of that for C_{ref}. However, to obtain the same magnitude of output ($\sqrt{|\nabla(E_{\mathrm{rms}})^2|}$) as that for the C_{ref} condition, the application of an electric field 1.56 (= 1/0.64) times stronger than that for the C_{ref} condition is needed because β is 36% smaller. Hence, the voltage must be 2.4 (= 1.56^2) times higher to induce the same dielectrophoretic force.

The difference between the results for C_{opt} and C_{ref} was primarily due to the opposing effects of frequency on the output and S/N ratio. Considering this trade-off effect, we sought for conditions that yield a higher output with an allowable S/N ratio by changing the frequency. Consequently, we found that a frequency of 300 kHz, which was between level 2 (200 kHz) and level 3 (400 kHz), resulted in a β value that was 27% higher than that obtained for C_{opt} at the expense of a somewhat smaller S/N ratio, which was 18.2 dB lower than that for C_{opt} (12.2% larger in variation) but 6.9 dB higher (54.9% lower) than that for C_{ref} (Table 5). Therefore, we recommend a frequency of 300 kHz for robust TTF treatment.

Conclusion

The optimum condition of TTF treatment with a high robustness to unpredictable variations in cell size and electrical properties was investigated by numerical simulations in which an AC voltage was applied to a mitotic cell. The magnitude of the dielectrophoretic force near the plane of cell division was evaluated for different voltages for combinations of six uncontrollable noise factors (cell membrane thickness, cell diameter, and electrical conductivities and relative permittivities of the intracellular fluid and cell membrane) and four controllable factors (frequency, electric field direction, and electrical conductivity and relative permittivity of the extracellular fluid). The number of simulation replicates needed for the combinations of these factors was reduced to 144 cases using the Taguchi method. Increasing the frequency significantly increased the robustness of the dielectrophoretic force irrespective of noise factors but

considerably decreased the magnitude of the force. Based on additional simulations that considered this trade-off effect, a frequency of 300 kHz is recommended for a robust TTF treatment with allowable variations. The dielectrophoretic force was almost independent of the angle of the applied electric field for deviations of ±20 degrees from the most effective direction. This study also demonstrated the effect of the electrical properties of the extracellular fluid, suggesting the feasibility of administrating saline as an exogenous solution to change the properties of the extracellular fluid. However, it should be noted that the MRI contrast agent used for imaging may have a negative effect on the TTF outcome.

Supporting information

S1 Fig. Geometric relationship between a cell and electrodes with angles of 20˚, 30˚, and 45˚.
(EPS)

S1 Table. List of parameters used in previous studies: Frequencies of applied electric field, cell geometry, and electrical properties of the cytoplasm, cell membrane and extracellular medium.
(PDF)

S2 Table. S/N ratio and β calculated by assigning noise factors and input M to L18 orthogonal array.
(PDF)

S3 Table. S/N ratio and β calculated by assigning control factors, compounded noise factors, and input M to L18 orthogonal array.
(PDF)

Author Contributions

Conceptualization: Kosaku Kurata, Hiroshi Takamatsu.

Data curation: Kosaku Kurata, Kazuki Shimada.

Formal analysis: Kosaku Kurata, Kazuki Shimada.

Funding acquisition: Kosaku Kurata.

Investigation: Kosaku Kurata, Kazuki Shimada.

Methodology: Kosaku Kurata, Hiroshi Takamatsu.

Project administration: Kosaku Kurata.

Resources: Kosaku Kurata.

Software: Kosaku Kurata, Kazuki Shimada.

Supervision: Kosaku Kurata, Hiroshi Takamatsu.

Validation: Kosaku Kurata.

Visualization: Kosaku Kurata, Kazuki Shimada.

Writing – original draft: Kosaku Kurata, Kazuki Shimada, Hiroshi Takamatsu.

Writing – review & editing: Kosaku Kurata, Kazuki Shimada, Hiroshi Takamatsu.

References

1. Kirson ED, Gurvich Z, Schneiderman R, Dekel E, Itzhaki A, Wasserman Y, et al. Disruption of cancer cell replication by alternating electric fields. Cancer Res. 2004; 64(9):3288–95. Epub 2004/05/06. https://doi.org/10.1158/0008-5472.can-04-0083 PMID: 15126372.
2. Kirson ED, Dbaly V, Tovarys F, Vymazal J, Soustiel JF, Itzhaki A, et al. Alternating electric fields arrest cell proliferation in animal tumor models and human brain tumors. Proc Natl Acad Sci U S A. 2007; 104 (24):10152–7. Epub 2007/06/07. https://doi.org/10.1073/pnas.0702916104 PMID: 17551011; PubMed Central PMCID: PMC1886002.
3. Stupp R, Wong ET, Kanner AA, Steinberg D, Engelhard H, Heidecke V, et al. NovoTTF-100A versus physician's choice chemotherapy in recurrent glioblastoma: a randomised phase III trial of a novel treatment modality. Eur J Cancer. 2012; 48(14):2192–202. Epub 2012/05/23. https://doi.org/10.1016/j.ejca.2012.04.011 PMID: 22608262.
4. Stupp R, Taillibert S, Kanner AA, Kesari S, Steinberg DM, Toms SA, et al. Maintenance Therapy With Tumor-Treating Fields Plus Temozolomide vs Temozolomide Alone for Glioblastoma: A Randomized Clinical Trial. JAMA. 2015; 314(23):2535–43. Epub 2015/12/17. https://doi.org/10.1001/jama.2015.16669 PMID: 26670971.
5. Stupp R, Taillibert S, Kanner A, Read W, Steinberg D, Lhermitte B, et al. Effect of Tumor-Treating Fields Plus Maintenance Temozolomide vs Maintenance Temozolomide Alone on Survival in Patients With Glioblastoma: A Randomized Clinical Trial. JAMA. 2017; 318(23):2306–16. Epub 2017/12/21. https://doi.org/10.1001/jama.2017.18718 PMID: 29260225; PubMed Central PMCID: PMC5820703.
6. Soni VS, Yanagihara TK. Tumor treating fields in the management of Glioblastoma: opportunities for advanced imaging. Cancer Imaging. 2019; 19(1):76. Epub 2019/12/01. https://doi.org/10.1186/s40644-019-0259-8 PMID: 31783910; PubMed Central PMCID: PMC6884888.
7. Wang Y, Pandey M, Ballo MT. Integration of Tumor-Treating Fields into the Multidisciplinary Management of Patients with Solid Malignancies. Oncologist. 2019; 24(12):e1426–e36. Epub 2019/08/25. https://doi.org/10.1634/theoncologist.2017-0603 PMID: 31444292; PubMed Central PMCID: PMC6975944.
8. Giladi M, Schneiderman RS, Porat Y, Munster M, Itzhaki A, Mordechovich D, et al. Mitotic disruption and reduced clonogenicity of pancreatic cancer cells in vitro and in vivo by tumor treating fields. Pancreatology. 2014; 14(1):54–63. Epub 2014/02/22. https://doi.org/10.1016/j.pan.2013.11.009 PMID: 24555979.
9. Giladi M, Schneiderman RS, Voloshin T, Porat Y, Munster M, Blat R, et al. Mitotic Spindle Disruption by Alternating Electric Fields Leads to Improper Chromosome Segregation and Mitotic Catastrophe in Cancer Cells. Sci Rep. 2015; 5:18046. Epub 2015/12/15. https://doi.org/10.1038/srep18046 PMID: 26658786; PubMed Central PMCID: PMC4676010.
10. Gera N, Yang A, Holtzman TS, Lee SX, Wong ET, Swanson KD. Tumor treating fields perturb the localization of septins and cause aberrant mitotic exit. PLoS One. 2015; 10(5):e0125269. Epub 2015/05/27. https://doi.org/10.1371/journal.pone.0125269 PMID: 26010837; PubMed Central PMCID: PMC4444126.
11. Kirson ED, Dbaly V, Tovarys F, Vymazal J, Soustiel JF, Itzhaki A, et al. Alternating electric fields arrest cell proliferation in animal tumor models and human brain tumors. Proc Natl Acad Sci U S A. 2007; 104 (24):10152–7. Epub 2007/06/07. https://doi.org/10.1073/pnas.0702916104 PMID: 17551011; PubMed Central PMCID: PMC1886002.
12. Harris CM, Kell DB. The radio-frequency dielectric properties of yeast cells measured with a rapid, automated, frequency-domain dielectric spectrometer. Journal of Electroanalytical Chemistry and Interfacial Electrochemistry. 1983; 156:15–28. https://doi.org/10.1016/S0022-0728(83)80648-2.
13. Hölzel R, Lamprecht I. Dielectric properties of yeast cells as determined by electrorotation. Biochimica et Biophysica Acta (BBA)—Biomembranes. 1992; 1104(1):195–200. https://doi.org/10.1016/0005-2736(92)90150-k PMID: 1550847
14. Hu X, Arnold WM, Zimmermann U. Alterations in the electrical properties of T and B lymphocyte membranes induced by mitogenic stimulation. Activation monitored by electro-rotation of single cells. Biochimica et Biophysica Acta (BBA)—Biomembranes. 1990; 1021(2):191–200. https://doi.org/10.1016/0005-2736(90)90033-k PMID: 2302395
15. Gascoyne PRC, Pethig R, Burt JPH, Becker FF. Membrane changes accompanying the induced differentiation of Friend murine erythroleukemia cells studied by dielectrophoresis. Biochimica et Biophysica Acta (BBA)—Biomembranes. 1993; 1149(1):119–26. https://doi.org/10.1016/0005-2736(93)90032-u PMID: 8318523
16. Arnold WM, Schmutzler RK, Schmutzler AG, van der Ven H, Al-Hasani S, Krebs D, et al. Electro-rotation of mouse oocytes: single-cell measurements of zona-intact and zona-free cells and of the isolated

zona pellucida. Biochimica et Biophysica Acta (BBA)—Biomembranes. 1987; 905(2):454–64. https://doi.org/10.1016/0005-2736(87)90475-5 PMID: 3689789

17. Sunderman FW. Measurement of Serum Total Base. Am J Clin Pathol. 1945; 15(6):219–22. https://doi.org/10.1093/ajcp/15.6.219

18. Sunderman FW. Rapid Measurement of Serum Total Base and Estimation of Serum Sodium: An Improved Conductivity Assembly. Am J Clin Pathol. 1949; 19(7):659–64. https://doi.org/10.1093/ajcp/19.7_ts.659 PMID: 18145455

19. Nörtemann K, Hilland J, Kaatze U. Dielectric Properties of Aqueous NaCl Solutions at Microwave Frequencies. The Journal of Physical Chemistry A. 1997; 101(37):6864–9. https://doi.org/10.1021/jp971623a

20. Gowrishankar TR, Stewart DA, Weaver JC. Model of a confined spherical cell in uniform and heterogeneous applied electric fields. Bioelectrochemistry. 2006; 68(2):181–90. Epub 2005/10/19. https://doi.org/10.1016/j.bioelechem.2005.07.002 PMID: 16230052.

21. Kotnik T, Bobanović F, Miklavc̆ic̆ D. Sensitivity of transmembrane voltage induced by applied electric fields—A theoretical analysis. Bioelectrochem Bioenerg. 1997; 43(2):285–91. https://doi.org/10.1016/S0302-4598(97)00023-8.

22. Kotnik T, Miklavcic D. Second-order model of membrane electric field induced by alternating external electric fields. IEEE Trans Biomed Eng. 2000; 47(8):1074–81. Epub 2000/08/16. https://doi.org/10.1109/10.855935 PMID: 10943056.

23. Kotnik T, Miklavcic D. Theoretical evaluation of voltage inducement on internal membranes of biological cells exposed to electric fields. Biophys J. 2006; 90(2):480–91. Epub 2005/10/22. https://doi.org/10.1529/biophysj.105.070771 PMID: 16239325; PubMed Central PMCID: PMC1367054.

24. Li X, Yang F, Rubinsky B. A Theoretical Study on the Biophysical Mechanisms by Which Tumor Treating Fields Affect Tumor Cells during Mitosis. IEEE Trans Biomed Eng. 2020. Epub 2020/01/16. https://doi.org/10.1109/TBME.2020.2965883 PMID: 31940516.

25. Stewart DA Jr., Gowrishankar TR, Smith KC, Weaver JC. Cylindrical cell membranes in uniform applied electric fields: validation of a transport lattice method. IEEE Trans Biomed Eng. 2005; 52(10):1643–53. Epub 2005/10/21. https://doi.org/10.1109/TBME.2005.856030 PMID: 16235650.

26. Tiwari PK, Kang SK, Kim GJ, Choi J, Mohamed AAH, Lee JK. Modeling of Nanoparticle-Mediated Electric Field Enhancement Inside Biological Cells Exposed to AC Electric Fields. Jpn J Appl Phys. 2009; 48(8):087001. https://doi.org/10.1143/jjap.48.087001

27. Wenger C, Giladi M, Bomzon Z, Salvador R, Basser PJ, Miranda PC. Modeling Tumor Treating Fields (TTFields) application in single cells during metaphase and telophase. Conf Proc IEEE Eng Med Biol Soc. 2015; 2015:6892–5. Epub 2016/01/07. https://doi.org/10.1109/EMBC.2015.7319977 PMID: 26737877.

28. Wenger C, Miranda PC, Salvador R, Thielscher A, Bomzon Z, Giladi M, et al. A Review on Tumor-Treating Fields (TTFields): Clinical Implications Inferred From Computational Modeling. IEEE Rev Biomed Eng. 2018; 11:195–207. Epub 2018/07/12. https://doi.org/10.1109/RBME.2017.2765282 PMID: 29993870.

29. Ye H, Cotic M, Fehlings MG, Carlen PL. Influence of cellular properties on the electric field distribution around a single cell. Progress In Electromagnetics Research B. 2012; 39:141–61. https://doi.org/10.2528/pierb11122705 pub.1070907814.

30. Ye H, Cotic M, Kang EE, Fehlings MG, Carlen PL. Transmembrane potential induced on the internal organelle by a time-varying magnetic field: a model study. J Neuroeng Rehabil. 2010; 7:12. Epub 2010/02/23. https://doi.org/10.1186/1743-0003-7-12 PMID: 20170538; PubMed Central PMCID: PMC2836366.

31. Fisher RA, Yates F. Statistical tables for biological, agricultural and medical research. Oxford, England: Oliver & Boyd; 1938. 90- p.

32. Taguchi G, Chowdhury S, Wu Y. Taguchi's Quality Engineering Handbook. Hoboken, New Jersey: John Wiley; 2005.

33. Abdelraof M, Hasanin MS, El-Saied H. Ecofriendly green conversion of potato peel wastes to high productivity bacterial cellulose. Carbohydr Polym. 2019; 211:75–83. Epub 2019/03/03. https://doi.org/10.1016/j.carbpol.2019.01.095 PMID: 30824106.

34. Saeedi Garakani S, Khanmohammadi M, Atoufi Z, Kamrava SK, Setayeshmehr M, Alizadeh R, et al. Fabrication of chitosan/agarose scaffolds containing extracellular matrix for tissue engineering applications. Int J Biol Macromol. 2020; 143:533–45. Epub 2019/12/10. https://doi.org/10.1016/j.ijbiomac.2019.12.040 PMID: 31816374.

35. Sathitkowitchai W, Nitisinprasert S, Keawsompong S. Improving palm kernel cake nutrition using enzymatic hydrolysis optimized by Taguchi method. 3 Biotech. 2018; 8(10):407. Epub 2018/09/22. https://doi.org/10.1007/s13205-018-1433-6 PMID: 30237954; PubMed Central PMCID: PMC6138002.

36. Savari M, Zarkesh Esfahani SH, Edalati M, Biria D. Optimizing conditions for production of high levels of soluble recombinant human growth hormone using Taguchi method. Protein Expr Purif. 2015; 114:128–35. Epub 2015/07/08. https://doi.org/10.1016/j.pep.2015.06.006 PMID: 26151869.

37. Sedighian H, Halabian R, Amani J, Heiat M, Taheri RA, Imani Fooladi AA. Manufacturing of a novel double-function ssDNA aptamer for sensitive diagnosis and efficient neutralization of SEA. Anal Biochem. 2018; 548:69–77. Epub 2018/03/03. https://doi.org/10.1016/j.ab.2018.02.017 PMID: 29496467.

38. Rockets Sullivan W., gauges, and pendulums: applying engineering principles to cell biology. Mol Biol Cell. 2019; 30(14):1635–40. Epub 2019/06/28. https://doi.org/10.1091/mbc.E19-02-0100 PMID: 31246543; PubMed Central PMCID: PMC6727760.

39. Kaushik A, Dwarakanath TA, Bhutani G. Robust Marker Detection and High Precision Measurement for Real-Time Anatomical Registration using Taguchi Method. Int J Med Robot. 2020:e2102. Epub 2020/03/13. https://doi.org/10.1002/rcs.2102 PMID: 32163657.

40. Ko C, Yang M, Byun T, Lee SW. Design factors of femur fracture fixation plates made of shape memory alloy based on the Taguchi method by finite element analysis. Int J Numer Method Biomed Eng. 2018; 34(5):e2967. Epub 2018/02/16. https://doi.org/10.1002/cnm.2967 PMID: 29447441.

41. Shie AJ, Lo KH, Lin WT, Juan CW, Jou YT. An integrated model using the Taguchi method and artificial neural network to improve artificial kidney solidification parameters. Biomed Eng Online. 2019; 18 (1):78. Epub 2019/07/07. https://doi.org/10.1186/s12938-019-0696-4 PMID: 31277654; PubMed Central PMCID: PMC6612084.

42. Sui J, Wang C, Sugita N. Experimental study of temperature rise during bone drilling process. Med Eng Phys. 2020. Epub 2020/02/12. https://doi.org/10.1016/j.medengphy.2020.01.007 PMID: 32044224.

43. Jones TB. Basic theory of dielectrophoresis and electrorotation. IEEE Eng Med Biol Mag. 2003; 22 (6):33–42. https://doi.org/10.1109/memb.2003.1304999 PMID: 15007989

44. Jones TB. Electromechanics of Particles: Cambridge University Press; 1995.

45. Ermolina I, Polevaya Y, Feldman Y, Ginzburg B, Schlesinger M. Study of normal and malignant white blood cells by time domain dielectric spectroscopy. IEEE Transactions on Dielectrics and Electrical Insulation. 2001; 8(2):253–61. https://doi.org/10.1109/94.919948

46. Joshi RP, Qin H, Schoenbach KH. Modeling studies of cell response to ultrashort, high-intensity electric fields-implications for intracellular manipulation. IEEE Transactions on Plasma Science. 2004; 32 (4):1677–86. https://doi.org/10.1109/TPS.2004.830971

47. Bomzon Z, Urman N, Wenger C, Giladi M, Weinberg U, Wasserman Y, et al. Modelling Tumor Treating Fields for the treatment of lung-based tumors. Conf Proc IEEE Eng Med Biol Soc. 2015; 2015:6888–91. Epub 2016/01/07. https://doi.org/10.1109/EMBC.2015.7319976 PMID: 26737876.

48. Mun EJ, Babiker HM, Weinberg U, Kirson ED, Von Hoff DD. Tumor-Treating Fields: A Fourth Modality in Cancer Treatment. Clin Cancer Res. 2018; 24(2):266–75. Epub 2017/08/03. https://doi.org/10.1158/1078-0432.CCR-17-1117 PMID: 28765323.

49. >Korshoej AR, Thielscher A, editors. Estimating the Intensity and Anisotropy of Tumor Treating Fields Jsing Singular Value Decomposition. Towards a More Comprehensive Estimation of Anti-tumor Efficacy. 2018 40th Annual International Conference of the IEEE Engineering in Medicine and Biology Society (EMBC); 2018 18–21 July 2018.

50. Korshoej AR, Sørensen JCH, von Oettingen G, Poulsen FR, Thielscher A. Optimization of tumor treating fields using singular value decomposition and minimization of field anisotropy. Phys Med Biol. 2019; 64(4):04NT3. https://doi.org/10.1088/1361-6560/aafe54 PMID: 30641498

51. Korshoej AR, editor Estimation of TTFields Intensity and Anisotropy with Singular Value Decomposition: A New and Comprehensive Method for Dosimetry of TTFields2019.

52. Ogunlade O, Beard P. Exogenous contrast agents for thermoacoustic imaging: An investigation into the underlying sources of contrast. Med Phys. 2015; 42(1):170–81. https://doi.org/10.1118/1.4903277 PMID: 25563258

53. Schneiderman RS, Giladi M, Porat Y, Munster M, Weinberg U, Kirson ED, et al. Overcoming cell size escape from tumor treating fields using a varying frequency treatment paradigm in vitro. J Clin Oncol. 2013; 31(15_suppl):e22134–e. https://doi.org/10.1200/jco.2013.31.15_suppl.e22134